



## Termination-II interstadial/stadial climate change recorded in two stalagmites from the north European Alps



Gina E. Moseley<sup>a,\*</sup>, Christoph Spötl<sup>a</sup>, Hai Cheng<sup>b,c</sup>, Ronny Boch<sup>a,d</sup>, Angela Min<sup>b</sup>, R. Lawrence Edwards<sup>b</sup>

<sup>a</sup> Institute of Geology, University of Innsbruck, Innrain 52, 6020 Innsbruck, Austria

<sup>b</sup> Department of Earth Sciences, University of Minnesota, 310 Pillsbury Drive SE, Minneapolis 55455, USA

<sup>c</sup> Institute of Global Environmental Change, Xi'an Jiaotong University, Xi'an, China

<sup>d</sup> Institute of Applied Geosciences, Graz University of Technology, Graz, Austria

### ARTICLE INFO

#### Article history:

Received 5 March 2015

Received in revised form

3 July 2015

Accepted 10 July 2015

Available online 31 July 2015

#### Keywords:

Speleothem

Termination II

Last interglacial

Millennial-scale climate change

Bølling/Allerød-Younger Dryas

Stable isotopes

U–Th dating

North Atlantic

Paleoclimatology

Quaternary

### ABSTRACT

Understanding the sequence of events that take place during glacial-interglacial climate transitions is important for improving our knowledge of abrupt climate change. Here, we present a new stacked, high-resolution, precisely-dated speleothem stable isotope record from the northern Alps, which provides an important record of temperature and moisture-source changes between 134 and 111 ka for Europe and the wider North Atlantic realm. The record encompasses the penultimate deglaciation (Termination II (TII)), which lies beyond the limit of radiocarbon dating, thus providing an important new archive for a crucial period of rapid paleoclimate change. Warmer and wetter ice-free conditions were achieved by  $134.1 \pm 0.7$  ka (modelled ages) as indicated by the presence of liquid water at the site. Temperatures warmed further at  $133.7 \pm 0.5$  ka and led into an interstadial, synchronous with slightly elevated monsoon strength during the week monsoon interval. The interstadial experienced an unstable climate with a trough in temperature associated with a slowdown in Atlantic Meridional Overturning Circulation (AMOC) and a reduction in North Atlantic Deep Water (NADW) formation. The interstadial ended with a more extreme cold reversal lasting 500 years in which NADW formation remained active but the sub-polar gyre weakened allowing cool polar waters to penetrate southwards. The main warming associated with TII was very rapid, taking place between  $130.9 \pm 0.9$  and  $130.7 \pm 0.9$  ka coeval with initial monsoon strengthening. Temperatures then plateaued before being interrupted by a 600-year cold event at  $129.1 \pm 0.6$  ka, associated once again with penetration of polar waters southwards into the North Atlantic and a slowdown in monsoon strengthening. Sub-orbital climate oscillations were thus a feature of TII in the north Atlantic realm, which broadly resemble the Bølling/Allerød-Younger Dryas-8.2 ka event pattern of change observed in Termination I despite monsoon records indicating strong differences between the last and penultimate deglaciation.

© 2015 The Authors. Published by Elsevier Ltd. This is an open access article under the CC BY-NC-ND license (<http://creativecommons.org/licenses/by-nc-nd/4.0/>).

### 1. Introduction

Investigations of the climate dynamics associated with glacial terminations and previous interglacial periods are important for addressing key questions associated with rapid warming and a future warmer climate (Denton et al., 2010; Stocker et al., 2013). The

last interglacial period (LIG), which roughly corresponds to the Eemian chronozone in Europe, is the best preserved of the previous interglacials in the geological record, and despite the difference in astronomical forcing compared to the present (Berger and Loutre, 1991; Berger and Yin, 2012), provides an important case study for a time when temperature was warmer (e.g., Bintanja et al., 2005; Kaspar et al., 2005; CAPE members, 2006), sea-level was higher (e.g., Kopp et al., 2009; Thompson et al., 2011; Dutton and Lambeck, 2012), and ice sheets were less extensive than today (e.g., Koerner, 1989; Otto-Bliesner et al., 2006; Alley et al., 2010; Stone et al., 2013).

The glacial termination (TII) preceding the last interglacial was a time of rapid climate change when ice sheets melted, sea level rose,

\* Corresponding author.

E-mail addresses: [gina.moseley@uibk.ac.at](mailto:gina.moseley@uibk.ac.at) (G.E. Moseley), [christoph.spötl@uibk.ac.at](mailto:christoph.spötl@uibk.ac.at) (C. Spötl), [cheng021@umn.edu](mailto:cheng021@umn.edu) (H. Cheng), [ronny.boch@tugraz.at](mailto:ronny.boch@tugraz.at) (R. Boch), [agm168@yahoo.com](mailto:agm168@yahoo.com) (A. Min), [edwar001@umn.edu](mailto:edwar001@umn.edu) (R.L. Edwards).

and atmospheric CO<sub>2</sub> concentrations increased (Denton et al., 2010). Drysdale et al. (2009) constrained the timing of the onset of TII as defined by the shift in Iberian-margin benthic  $\delta^{18}\text{O}$  towards interglacial values to  $141 \pm 2.5$  ka, by linking northwest Italian speleothem  $\delta^{18}\text{O}$  to Iberian-margin sea surface temperatures (SST). In contrast, Cheng et al. (2006) linked the record of monsoon  $\delta^{18}\text{O}$  to North Atlantic ice rafted debris (IRD) records and found that Iberian-margin benthic  $\delta^{18}\text{O}$  began to shift at the beginning of the week monsoon interval dated to  $135.5 \pm 1.0$  ka. Some discrepancy thus exists regarding the onset of marine TII. The ensuing release of large amounts of meltwater and icebergs into the oceans, especially the northern North Atlantic Ocean, had the effect of cooling SSTs (Waelbroeck et al., 2008), thereby reducing the Atlantic Meridional Overturning Circulation (AMOC) and the associated northward transport of heat (McManus et al., 2004), which further resulted in a weakened Asian monsoon (Cheng et al., 2006, 2009). Recovery of the climate system began in response to strengthening of the AMOC and resumption of North Atlantic Deep Water (NADW) formation (Waelbroeck et al., 2008; Drysdale et al., 2009). Unfortunately, unlike the last deglaciation which began c.20,000 years ago, the timing of this sequence of events during TII, and the corresponding terrestrial response, is less well understood because it lies beyond the limit of radiocarbon dating, and thus is lacking in reliably-dated archives upon which understanding of rapid climate change can be improved.

Previous studies have shown that  $\delta^{18}\text{O}$  records of speleothem calcite from the Northern Alps (NALPS) are strongly influenced by climatic changes in the North Atlantic realm. In particular, the similarities between the NALPS  $\delta^{18}\text{O}$  records and winter-dominated (Denton et al., 2005) Greenland  $\delta^{18}\text{O}$  records across rapid millennial-scale climate-change events associated with glacial stadial–interstadial transitions are remarkable (Boch et al., 2011; Moseley et al., 2014; Luetscher et al., 2015), whilst  $\delta^{18}\text{O}$  signatures from Spannagel cave speleothems mimic the Holocene North Atlantic pattern of ocean surface hydrography (Bond et al., 2001; Mangini et al., 2007). Such results imply a common forcing acted during both the last glacial and current interglacial periods to link the climates of Greenland and central Europe. In this study, we utilize this strong connection that exists between the North Atlantic region and central Europe during abrupt warmings, and address the need for more reliably-dated terrestrial paleoclimate archives from the sensitive North Atlantic region that cover TII and the LIG by extending the high-resolution NALPS  $\delta^{18}\text{O}$  speleothem record (Boch et al., 2011; Moseley et al., 2014) back to c. 134 ka.

## 2. Methods

### 2.1. Regional climate

Back-trajectory studies indicate that under contemporary conditions, the northern Alps receives 44% of its annual moisture from the North Atlantic Ocean, whilst 17% originates in the Mediterranean Sea, 21% from land evaporation, 13% from the North and Baltic seas, and 5% from the Arctic and Nordic seas (Sodemann and Zubler, 2010). Seasonally, the North Atlantic Ocean contributes the majority of moisture during winter and summer. In summer, contributions from the North Atlantic Ocean are much reduced and land evaporation contributes the most precipitation. Autumn precipitation moisture sources are split between the North Atlantic Ocean and Mediterranean Sea (Sodemann and Zubler, 2010). For a given altitude, the  $\delta^{18}\text{O}$  composition of precipitation originating in the North Atlantic Ocean will be more depleted than for a Mediterranean source, both as a result of the source waters being more depleted in the North Atlantic Ocean, and also the longer transport

pathway and successive rainout of the North Atlantic moisture (Kaiser et al., 2002).

### 2.2. Cave sites and stalagmites

Schneckenloch is a cave formed in the Lower Cretaceous Schraffenkalk Formation on the northern rim of the European Alps (Fig. 1), Austria, with an entrance elevation of 1285 m a.s.l., a total passage length of 3.5 km, and a constant interior cave air temperature of c. 6 °C. Mean annual precipitation is 1908 mm (1971–2000; Schopperrau; 835 m a.s.l.; 7 km away; the weighted mean annual  $\delta^{18}\text{O}$  value is  $-10.8\text{‰}$  (Humer et al., 1995)) and vegetation cover includes open spruce forest. Stalactites are actively forming in the cave today, but modern stalagmite and flowstone deposition appears to be largely absent. A c. 33 cm candlestick-type stalagmite, SCH-5 (Fig. 2), was collected in situ c. 400 m from the cave entrance. The catchment above the gallery where SCH-5 was recovered from is c. 1450 m a.s.l. Using an altitude gradient of  $-0.16\text{‰}$   $100 \text{ m}^{-1}$  (Lauber and Goldscheider, 2014), we calculate from the Schopperrau data the modern  $\delta^{18}\text{O}$  composition of the drip water at the location of SCH-5 as  $-11.8\text{‰}$ .

SCH-5 was found partly buried beneath laminated clay-rich silt that was presumably deposited during back-flooding of the cave when ice blocked the cave's drainage during the Last Glacial Maximum. The surface of the stalagmite is heavily corroded attesting to the interaction with calcite-undersaturated water after its formation. A slab taken from the central axis of SCH-5 shows that the outermost layer probably also underwent some post-depositional alteration producing an opaque spikey texture. The interior of the sample however, is pristine, composed of dense calcite with a tanned color, and lacks macroscopic hiatuses (Fig. 2).

Hölloch is a cave located in the same host rock as Schneckenloch, c.10 km to the east (Fig. 1), and at a similar altitude (1240–1438 m a.s.l.). The cave is 10.9 km in length, and maintains a constant temperature of  $5.6 \pm 0.2$  °C (Spötl et al., 2011). The catchment above the cave is c. 1450 m a.s.l., thus the modern  $\delta^{18}\text{O}$  composition of the drip water is calculated as  $-11.6\text{‰}$ . The  $\delta^{18}\text{O}$  values of mean winter and summer precipitation in this area are c.  $-14\text{‰}$ , and  $-8.6\text{‰}$ , respectively (Field, 2010).

HÖL-10 was found broken, probably as a result of flooding, in the southern part of the system. The recovered sample is present in seven parts that can easily be placed into stratigraphic order yielding a candlestick-type stalagmite that is c. 126 cm in length. The top of the sample is missing, but the base is complete, and it is the bottom c. 11.5 cm (Fig. 3) that were analyzed in this study.

### 2.3. Analytical methods

SCH-5 and HÖL-10 were both analyzed for U and Th concentrations, isotopic ratios, and age data, as well as stable isotopes. Sub-samples of 30–80 mg were hand drilled along specific growth layers for U–Th analysis (SCH-5,  $n = 23$ ; HÖL-10,  $n = 13$ ). Chemical separation and multi-collector inductively-coupled-plasma mass-spectrometric (Finnigan Neptune) measurements of U and Th isotope ratios were produced using state-of-the-art facilities and the latest protocols at the University of Minnesota (Shen et al., 2012; Cheng et al., 2013). The age datum is 1950 A.D. (Table 1).

For stable isotope analyses ( $\delta^{18}\text{O}$  and  $\delta^{13}\text{C}$ ), a total of 2178 powders were micro-milled at a spatial resolution of 0.15 mm from the central axis of SCH-5, and 419 powders at a resolution of 0.25 mm from the central axis of the basal segment of HÖL-10, and measured on a Thermo Fisher Delta<sup>plus</sup>XL isotope ratio mass spectrometer linked to a Gasbench II at the University of Innsbruck. All isotope results are reported relative to the Vienna PeeDee



**Fig. 1.** Location of sites discussed in text. (1) Schneckenloch cave and Hölloch cave, this study. (2) Spannagel cave (Holzkämper et al., 2004, 2005). (3) Entrische Kirche cave (Meyer et al., 2008). (4) Corchia cave (Drysdale et al., 2005, 2009). (5) NEEEM ice core (NEEM community members, 2013). (6) Iberian Margin, MD95-2042 and MD01-2444 (Drysdale et al., 2009 and references therein). (7) Iberian Margin, MD99-2331 (Gouzy et al., 2004 and references therein). (8) Bay of Biscay, MD04-2845 (Sánchez Goñi et al., 2008). (9) Lago Grande di Monticchio maar lake (Brauer et al., 2007). (10) Sanbao Cave (Wang et al., 2008; Cheng et al., 2009). Map adapted from FreeVectorMaps.com.

Belemnite standard. Analytical precisions are 0.08‰ and 0.06‰ for  $\delta^{18}\text{O}$  and  $\delta^{13}\text{C}$  respectively ( $1\sigma$ ) (Spötl, 2011).

Age models (Fig. 4) were constructed for both SCH-5 and HÖL-10 using OxCal version 4.2 for depositional models (Bronk Ramsey, 2008; Bronk Ramsey and Lee, 2013), with a variable “k” parameter of 0.001–10  $\text{mm}^{-1}$  (Bronk Ramsey and Lee, 2013).

Thin sections were prepared for the basal section of SCH-5, specifically to investigate the crystal fabric and continuity across the color change c. 300 mm from the top of the stalagmite (Fig. 2).

### 3. Results

The calcite of SCH-5 and HÖL-10 yields  $^{238}\text{U}$  concentrations between 0.2–1.1  $\mu\text{g g}^{-1}$  and 0.5–1.3  $\mu\text{g g}^{-1}$  respectively, with measured  $(^{230}\text{Th}/^{232}\text{Th})_{\text{atomic}}$  ranging from 1,300 to  $53,300 \times 10^{-6}$  and 230 to  $23,200 \times 10^{-6}$  respectively. Given the generally low presence of detrital Th within the samples, we adopt an *a priori* correction for initial  $^{230}\text{Th}/^{232}\text{Th}$  based on the bulk-Earth  $(^{230}\text{Th}/^{232}\text{Th})_{\text{atomic}}$  of  $4.4 \pm 2.2 \times 10^{-6}$  (Wedepohl, 1995). Differences in uncorrected and corrected U-Th ages are small (Table 1). U-Th dates are precise, with 89% of ages yielding a precision of 0.3–0.6%, and 11% yielding a precision of 0.9–1.4%. All ages are in stratigraphic order within  $2\sigma$  uncertainty (Table 1). The temporal resolution of the final modelled stable isotope interval averages 9 yrs (range <1–145 yrs) for SCH-5, and continuously covers the period  $115.3 \pm 0.6$  to  $134.1 \pm 0.7$  ka (modelled ages), whilst the average temporal interval for HÖL-10 is 50 yrs (range 5–163 yrs) and covers the interval  $110.8 \pm 2.5$  to  $131.8 \pm 1.2$  ka (modelled ages). The  $\delta^{18}\text{O}$  records from SCH-5 and HÖL-10 both vary between a minimum of c. –11‰, and maximum of c. –8‰ (Fig 5a). In contrast, the absolute values and amplitude of change in the respective  $\delta^{13}\text{C}$

records are quite different, with SCH-5 varying between c. 4 and –4‰, whilst HÖL-10 varies between c. 0 and –6‰ (Fig. 5b).  $\delta^{18}\text{O}$  and  $\delta^{13}\text{C}$  values are moderately correlated in SCH-5 ( $r^2 = 0.6$ ), and poorly correlated in HÖL-10 ( $r^2 < 0.1$ ). Growth rates are also highly variable; SCH-5 exhibits fairly fast deposition between 1 and 188  $\text{mm ka}^{-1}$ , whilst HÖL-10 grew at a rate of 2–50  $\text{mm ka}^{-1}$  (Fig 5c). The rate of 50  $\text{mm ka}^{-1}$  is however a product of the treatment of the displaced age at 1246 mm by the age modelling software (Fig. 4). The correlation between growth rate and  $\delta^{18}\text{O}$ , or growth rate and  $\delta^{13}\text{C}$  in both samples is very poor ( $r^2 < 0.1$ ) in all cases.

Thin-section analysis of the crystal fabric across the color change c. 300 mm from the top of the stalagmite (Fig. 2) demonstrated uninterrupted crystal growth and no evidence of a (micro) hiatus (Fig. 6). Any isotopic changes across this color-change boundary are thus a genuine feature of the SCH-5 isotopic record and not the result of a hiatus.

### 4. Discussion

Between c. 132 to 119 ka, changes in the two  $\delta^{18}\text{O}$  records are synchronous within the level of 2-sigma uncertainty as highlighted by the horizontal bars in Fig. 5a. Absolute values for HÖL-10 appear to be slightly more extreme than for SCH-5, i.e., for periods of high or increasing  $\delta^{18}\text{O}$ , HÖL-10 is marginally more enriched than SCH-5, whilst during low or decreasing periods of  $\delta^{18}\text{O}$ , HÖL-10 is marginally more depleted than SCH-5 indicating some buffering of the signal in SCH-5. Furthermore, the SCH-5 signal is noisier than HÖL-10 as a result of the higher resolution of the record and also the much faster and variable growth rate of SCH-5 (Fig. 5c), which would be more responsive to changes in  $\delta^{18}\text{O}$  of the drip water than the slower diffuse flow of HÖL-10 (cf. Baldini et al., 2006). Given the reproducibility (Dorale and Liu, 2009) of the two  $\delta^{18}\text{O}$  records over the period 132 to 119 ka, which grew in close proximity to one another and at the same altitude, plus the lack of correlation between  $\delta^{18}\text{O}$  and  $\delta^{13}\text{C}$  in both samples (Hendy, 1971), the changes in  $\delta^{18}\text{O}$  recorded in the speleothems are considered to represent at least regional variations in the  $\delta^{18}\text{O}$  of precipitation rather than in-cave or vadose-zone processes. In contrast, the  $\delta^{13}\text{C}$  records that have been reconstructed from the two samples are vastly different in terms of absolute values, amplitudes of change, and direction of change (Fig. 5b), thus given the complications of understanding this proxy, we do not rely too heavily on it in the following interpretation.

The  $\delta^{18}\text{O}$  records demonstrate a two-phase pattern in which the period prior to c. 125 ka displays an oscillating, step-wise rise from c. –11 to –8‰ that tracks Northern Hemisphere summer insolation (Fig. 7), whilst the period between 125 and 119 ka is rather stable (Fig. 7). The enrichment in  $^{18}\text{O}$  up to c. 125 ka followed by relatively stable conditions to c. 119 ka is comparable to the timing and pattern of shifts in  $\delta^{18}\text{O}$  recorded in speleothems from the eastern Alps (Meyer et al., 2008) and higher elevation (2200–2500 m a.s.l.) central Alps (Fig. 7d) (Holzkämper et al., 2004, 2005). The c. 1–1.5 ‰ depletion in  $\delta^{18}\text{O}$  at the higher elevation sites can be accounted for by taking into account the altitude difference (–0.16‰  $100 \text{ m}^{-1}$ ; Lauber and Goldscheider, 2014). In contrast, the eastern Alpine Entrische Kirche cave is at a lower elevation (1040 m a.s.l.) compared to the two sites studied here, but is further inland, thus lower  $\delta^{18}\text{O}$  values may be due to the longer transport pathway and progressive rainout of  $^{18}\text{O}$ .

Following c. 119 ka, the respective  $\delta^{18}\text{O}$  signals deviate from one another: HÖL-10, which displayed comparable absolute  $\delta^{18}\text{O}$  values to SCH-5 between c. 132–119 ka, shows a subdued depletion in  $\delta^{18}\text{O}$  that is consistent with the  $\delta^{18}\text{O}$  signal from another Schneckenloch speleothem dated in the same laboratory (SCH-7) (Fig. 7c) (Boch



**Fig. 2.** SCH-5, c. 33 cm in length, showing an outer opaque spikey texture (right) probably as a result of some post-depositional alteration. The interior of the sample (left) is pristine in the center and composed of dense calcite with a tanned color and lacks macroscopic hiatuses. A color change is marked at the bottom for which thin sections were prepared to investigate the crystal fabric and continuity. “AZ” refers to the potentially altered zone on the flanks of the sample discussed in the text. Numbers indicate the position in the sample of: 1. The initial rise in  $\delta^{18}\text{O}$  at the beginning of the TII-interstadial; 2. The beginning of the decrease in  $\delta^{18}\text{O}$  that marks the end of the TII-interstadial, and; 3. The main abrupt rise in  $\delta^{18}\text{O}$  associated with the glacial-interglacial transition, which is also coincident with a color change in the speleothem fabric.

et al., 2011), and also with the timing of a marked depletion in  $\delta^{18}\text{O}$  in the eastern Alpine speleothem record (Fig. 7d) (Meyer et al., 2008). By contrast, the  $\delta^{18}\text{O}$  record of SCH-5 remains relatively stable and similar to mid-late LIG values recorded earlier in the stalagmite (Fig. 7). We do not fully understand why  $\delta^{18}\text{O}$  in SCH-5 does not shift to lower values following 119 ka, especially given that another sample from the same cave does record the shift. If the opposing signals are a true reflection of the  $\delta^{18}\text{O}$  of the feeding drip waters at that time, it could be related to different flow paths towards the different drip sites (Smart and Friederich, 1986) and a sensitivity to changes in precipitation seasonality (Baker et al., 1997; Baldini et al., 2006). In addition, we note that the amplitude of the depletion in  $\delta^{18}\text{O}$  recorded in the eastern Alpine speleothem beginning at c. 119 ka is more extreme than the NALPS speleothems (Fig. 7). The catchment area for Entrische Kirche cave is today unglaciated, however, during past glacial episodes two ice streams flowed from the main alpine crest, covering most of the catchment (van Husen, 1987; Meyer et al., 2008). Given the proneness of the site for glaciation, we attribute the sharp marked



**Fig. 3.** The interior slab of the base of HÖL-10, c. 11.5 cm in length. Numbers indicate the position in the sample of: 1. The beginning of the decrease in  $\delta^{18}\text{O}$  that marks the end of the TII-interstadial, and; 2. The main abrupt rise in  $\delta^{18}\text{O}$  associated with the glacial-interglacial transition.

depletion in  $\delta^{18}\text{O}$  of Entrische Kirche cave to an increase in snowfall and glacier expansion at the glacial inception, both of which would result in a depletion in the  $\delta^{18}\text{O}$  of waters (Sodemann, 2006) recharging the epikarst.

In the following discussion, we focus our interpretation on the main period of climate change between 134 and 125 ka and use SCH-5 as our “master” record, since it has the higher overall growth rate of the two samples (Fig. 5c) thus enabling it to record sub-orbital climate events at higher resolution. SCH-5 has also been analyzed with more U–Th anchor points, at higher resolution, and at higher precision than HÖL-10.

#### 4.1. Termination II in central Europe

The new  $\delta^{18}\text{O}$  speleothem records presented here appear to record changing values in the isotopic composition of precipitation over TII. Under modern conditions, the  $\delta^{18}\text{O}$  composition of cave drip waters at these two sites is considered to be a mixed seasonal signal reflecting the mean annual  $\delta^{18}\text{O}$  of precipitation, though some evaporative loss is expected during summer resulting in a slightly reduced input of summer recharge to the epikarst. The transfer of precipitation to the drip site is expected to be a matter of weeks, similar to the nearby Bärenhöhle where a 3 year monitoring programme has taken place (Luetscher et al., 2014). Today, temporal variations in the  $\delta^{18}\text{O}$  composition of precipitation in the

**Table 1**  
MC-ICP-MS U–Th dating results of Schneckloch and Hölloch speleothems.

Sample (mm dft)	$^{238}\text{U}$ [ng g $^{-1}$ ]	$^{232}\text{Th}$ [pg g $^{-1}$ ]	$^{230}\text{Th}/^{232}\text{Th}$ (atomic $\times 10^{-6}$ )	$\delta^{234}\text{U}^a$ (measured)	$^{230}\text{Th}/^{238}\text{U}^b$ (activity)	Uncorrected age (a) $^c$	Corrected age (a) $^d$	$\delta^{234}\text{U}^a$ (initial)
<b>SCH-5</b>								
8.9	357 $\pm$ 1	2328 $\pm$ 47	2281 $\pm$ 46	329 $\pm$ 2	0.9016 $\pm$ 0.0018	115790 $\pm$ 531	115595 $\pm$ 538	456 $\pm$ 3
14.1	841 $\pm$ 1	374 $\pm$ 8	34035 $\pm$ 698	345 $\pm$ 2	0.9194 $\pm$ 0.0017	117045 $\pm$ 464	116973 $\pm$ 464	480 $\pm$ 2
17.9	506 $\pm$ 1	168 $\pm$ 4	44921 $\pm$ 960	322 $\pm$ 2	0.9058 $\pm$ 0.0015	117880 $\pm$ 454	117813 $\pm$ 454	448 $\pm$ 3
22.4	1052 $\pm$ 1	382 $\pm$ 8	42466 $\pm$ 873	355 $\pm$ 2	0.9359 $\pm$ 0.0015	119033 $\pm$ 435	118962 $\pm$ 435	496 $\pm$ 2
41.1	845 $\pm$ 1	246 $\pm$ 6	53303 $\pm$ 1220	351 $\pm$ 2	0.9393 $\pm$ 0.0023	120400 $\pm$ 635	120330 $\pm$ 635	493 $\pm$ 3
77.1	453 $\pm$ 1	299 $\pm$ 6	22879 $\pm$ 494	324 $\pm$ 2	0.9180 $\pm$ 0.0017	120352 $\pm$ 515	120275 $\pm$ 515	454 $\pm$ 3
107.1	427 $\pm$ 1	481 $\pm$ 10	13507 $\pm$ 282	325 $\pm$ 2	0.9241 $\pm$ 0.0018	121443 $\pm$ 538	121356 $\pm$ 539	458 $\pm$ 3
141.6	302 $\pm$ 0.3	324 $\pm$ 7	14166 $\pm$ 306	319 $\pm$ 2	0.9227 $\pm$ 0.0015	122207 $\pm$ 470	122122 $\pm$ 470	450 $\pm$ 2
158.9	478 $\pm$ 1	290 $\pm$ 6	25669 $\pm$ 546	335 $\pm$ 1	0.9435 $\pm$ 0.0015	124175 $\pm$ 426	124099 $\pm$ 426	475 $\pm$ 2
163.4	271 $\pm$ 0.3	616 $\pm$ 12	6773 $\pm$ 137	322 $\pm$ 1	0.9348 $\pm$ 0.0013	124431 $\pm$ 412	124321 $\pm$ 413	458 $\pm$ 2
170.9	405 $\pm$ 1	636 $\pm$ 13	9876 $\pm$ 201	330 $\pm$ 2	0.9411 $\pm$ 0.0016	124449 $\pm$ 494	124354 $\pm$ 494	469 $\pm$ 3
180.6	379 $\pm$ 0.4	279 $\pm$ 6	20810 $\pm$ 437	315 $\pm$ 2	0.9303 $\pm$ 0.0017	124779 $\pm$ 510	124700 $\pm$ 510	448 $\pm$ 3
211.4	399 $\pm$ 1	198 $\pm$ 5	31284 $\pm$ 725	326 $\pm$ 2	0.9399 $\pm$ 0.0017	124878 $\pm$ 504	124804 $\pm$ 504	464 $\pm$ 3
227.1	373 $\pm$ 1	670 $\pm$ 14	8550 $\pm$ 176	311 $\pm$ 2	0.9312 $\pm$ 0.0018	125739 $\pm$ 555	125638 $\pm$ 556	443 $\pm$ 3
257.9	487 $\pm$ 1	350 $\pm$ 8	21485 $\pm$ 463	312 $\pm$ 2	0.9358 $\pm$ 0.0016	126562 $\pm$ 516	126484 $\pm$ 516	446 $\pm$ 3
272.1	499 $\pm$ 1	259 $\pm$ 6	30297 $\pm$ 672	332 $\pm$ 2	0.9552 $\pm$ 0.0016	127506 $\pm$ 498	127434 $\pm$ 498	475 $\pm$ 3
284.1	726 $\pm$ 1	833 $\pm$ 17	13724 $\pm$ 277	329 $\pm$ 2	0.9560 $\pm$ 0.0020	128137 $\pm$ 583	128051 $\pm$ 583	473 $\pm$ 3
290.9	249 $\pm$ 1	400 $\pm$ 8	9882 $\pm$ 208	344 $\pm$ 7	0.9640 $\pm$ 0.0050	127308 $\pm$ 1736	127212 $\pm$ 1736	492 $\pm$ 10
294.2	221 $\pm$ 0.2	653 $\pm$ 13	5451 $\pm$ 111	349 $\pm$ 2	0.9790 $\pm$ 0.0017	129767 $\pm$ 550	129648 $\pm$ 551	504 $\pm$ 3
302.1	304 $\pm$ 0.3	1733 $\pm$ 35	2994 $\pm$ 60	407 $\pm$ 2	1.0347 $\pm$ 0.0018	131905 $\pm$ 552	131738 $\pm$ 556	590 $\pm$ 3
304.4	739 $\pm$ 1	2826 $\pm$ 57	4456 $\pm$ 90	400 $\pm$ 2	1.0037 $\pm$ 0.0019	132931 $\pm$ 561	132797 $\pm$ 563	582 $\pm$ 3
310.3	699 $\pm$ 1	6981 $\pm$ 140	1704 $\pm$ 34	394 $\pm$ 2	1.0321 $\pm$ 0.0018	133645 $\pm$ 573	133398 $\pm$ 587	574 $\pm$ 3
313.3	480 $\pm$ 1	6194 $\pm$ 124	1298 $\pm$ 26	372 $\pm$ 2	1.0164 $\pm$ 0.0017	133890 $\pm$ 569	133585 $\pm$ 593	545 $\pm$ 3
<b>HÖL-10</b>								
1182.00	1171 $\pm$ 1	714 $\pm$ 15	21825 $\pm$ 446	206 $\pm$ 2	0.8076 $\pm$ 0.0015	115406 $\pm$ 461	115328 $\pm$ 461	285 $\pm$ 2
1196.25	1178 $\pm$ 1	685 $\pm$ 14	23192 $\pm$ 468	211 $\pm$ 2	0.8178 $\pm$ 0.0013	117051 $\pm$ 453	116978 $\pm$ 453	293 $\pm$ 2
1202.25	867 $\pm$ 1	6560 $\pm$ 131	1754 $\pm$ 35	183 $\pm$ 2	0.8046 $\pm$ 0.0014	119078 $\pm$ 490	118842 $\pm$ 504	256 $\pm$ 2
1207.25	699 $\pm$ 1	10009 $\pm$ 200	977 $\pm$ 20	228 $\pm$ 2	0.8479 $\pm$ 0.0014	121205 $\pm$ 495	120829 $\pm$ 541	321 $\pm$ 3
1220.00	904 $\pm$ 1	31074 $\pm$ 622	401 $\pm$ 8	195 $\pm$ 2	0.8353 $\pm$ 0.0014	124682 $\pm$ 520	123832 $\pm$ 758	277 $\pm$ 2
1231.75	867 $\pm$ 4	2411 $\pm$ 49	5008 $\pm$ 104	208 $\pm$ 4	0.8446 $\pm$ 0.0052	124440 $\pm$ 1614	124317 $\pm$ 1613	295 $\pm$ 6
1239.00	1281 $\pm$ 2	2679 $\pm$ 54	6491 $\pm$ 131	177 $\pm$ 2	0.8232 $\pm$ 0.0016	125279 $\pm$ 587	125166 $\pm$ 588	252 $\pm$ 3
1246.00	1327 $\pm$ 1	7203 $\pm$ 144	2586 $\pm$ 52	194 $\pm$ 1	0.8513 $\pm$ 0.0012	129301 $\pm$ 465	129114 $\pm$ 472	279 $\pm$ 2
1249.00	1278 $\pm$ 1	3904 $\pm$ 78	4626 $\pm$ 93	204 $\pm$ 1	0.8567 $\pm$ 0.0013	128575 $\pm$ 473	128442 $\pm$ 475	293 $\pm$ 2
1250.00	1137 $\pm$ 1	3431 $\pm$ 69	4688 $\pm$ 94	205 $\pm$ 1	0.8580 $\pm$ 0.0013	128728 $\pm$ 468	128596 $\pm$ 470	294 $\pm$ 2
1253.00	829 $\pm$ 0.9	11100 $\pm$ 222	1060 $\pm$ 21	208 $\pm$ 2	0.8609 $\pm$ 0.0014	128856 $\pm$ 541	128495 $\pm$ 579	299 $\pm$ 2
1255.00	Isochron			207 $\pm$ 5	0.8651 $\pm$ 0.0040		130100 $\pm$ 1600	299 $\pm$ 6
1258.50	543 $\pm$ 0.6	33076 $\pm$ 663	234 $\pm$ 5	195 $\pm$ 2	0.8636 $\pm$ 0.0016	132615 $\pm$ 629	131160 $\pm$ 1163	282 $\pm$ 3

dft = distance from top.

All uncertainties are  $2\sigma$ .

$$^a \delta^{234}\text{U} = \left( \frac{^{234}\text{U}/^{238}\text{U}}{\text{activity}} - 1 \right) \times 1000.$$

$$^b \left[ \frac{^{230}\text{Th}}{^{238}\text{U}} \right]_{\text{activity}} = 1 - e^{-\lambda_{230}T} + \left( \frac{\delta^{234}\text{U}_{\text{measured}}}{1000} \right) \left[ \frac{\lambda_{230}}{\lambda_{230} - \lambda_{234}} \right] \left( 1 - e^{-(\lambda_{230} - \lambda_{234})T} \right), \text{ where } T \text{ is age in years. } \lambda_{230} = 9.1705 \times 10^{-6} \text{ a}^{-1} \text{ (Cheng et al., 2013),}$$

$$\lambda_{234} = 2.8221 \times 10^{-6} \text{ a}^{-1} \text{ (Cheng et al., 2013), } \lambda_{238} = 1.551 \times 10^{-10} \text{ a}^{-1} \text{ (Jaffey et al., 1971).}$$

$^c$  Years before measurement and without detrital Th correction.

$^d$  Years before 1950 A.D.. Corrected for detrital Th contamination using the bulk earth atomic value of  $4.4 \pm 2.2$  ppm for initial  $^{230}\text{Th}/^{232}\text{Th}_{\text{act}}$  (Wedepohl, 1995). The degree of detrital  $^{230}\text{Th}$  contamination is indicated by the measured ( $^{230}\text{Th}/^{232}\text{Th}$ ) activity ratio.

northern Alps are highly correlated to changes in air temperature, the amount of precipitation, and the North Atlantic Oscillation (NAO) (particularly during winter) (Kaiser et al., 2002; Schürch et al., 2003; Field, 2010). Changes in the  $\delta^{18}\text{O}$  of speleothem calcite have thus previously been considered to be controlled primarily by mean annual temperature, with higher (lower)  $\delta^{18}\text{O}$  reflecting warmer (cooler) periods over orbital and millennial timescales (Boch et al., 2011; Moseley et al., 2014). The major shifts in  $\delta^{18}\text{O}$  in our new record are also likely to be temperature controlled, but exacerbated by changes in the relative contributions of different moisture sources and the seasonal distribution of meteoric precipitation. For instance, southward shifts in the polar front during stadials and glacials (Sánchez Goñi et al., 1999) resulted not only in a regional decline in air temperature (depleting  $\delta^{18}\text{O}$ ), but also reduced advection across the Mediterranean (Drysdale et al., 2009). Thus, the input of heavier  $\delta^{18}\text{O}$  Mediterranean-sourced moisture (LeGrande and Schmidt, 2006) with a shorter transport pathway to NALPS speleothems would have been reduced relative to North Atlantic Ocean-sourced moisture during cold events. The opposite would have occurred during warm events in which  $^{18}\text{O}$  was enriched both through

higher temperatures and also due to an increase in the ratio of Mediterranean-sourced moisture relative to North Atlantic Ocean-sourced moisture. By contrast, the amount effect is not thought to be a factor that influences the  $\delta^{18}\text{O}$  of NALPS speleothems, because it works in the opposite direction to that which is recorded i.e. drier conditions during cool events would increase the  $\delta^{18}\text{O}$  of precipitation.

Large influxes of meltwater and icebergs streamed into the North Atlantic Ocean following the onset of TII resulting in a major peak in IRD known as Heinrich 11 (e.g., Heinrich, 1988; Bond et al., 1992; McManus et al., 1994, 1998; Drysdale et al., 2009). Such large influxes of freshwater have the effect of stratifying surface waters (Bauch et al., 2000; Denton et al., 2010) and reducing NADW formation (Heinrich, 1988; Bond et al., 1992; McManus et al., 1999), which in turns leads to an expansion of winter sea ice and a highly seasonal winter climate in the North Atlantic realm (Denton et al., 2005, 2010).

Initiation of speleothem growth at Spannagel cave ( $136.7 \pm 2.8$  ka) located in the high-elevation central Alps (Holzkämper et al., 2005) and Schneckloch cave ( $134.1 \pm 0.7$  ka) studied here, indicates that the climate had

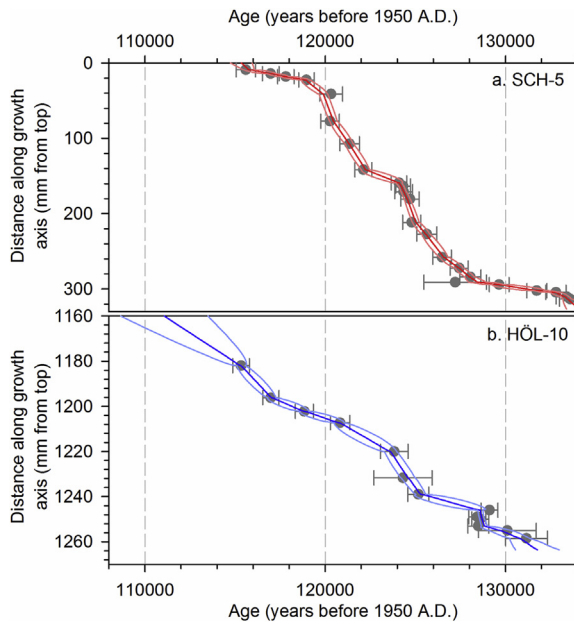


**Fig. 4.** OxCal age models (Bronk Ramsey, 2008; Bronk Ramsey and Lee, 2013) for the two speleothems presented in this study: (a) SCH-5; (b) HÖL-10.

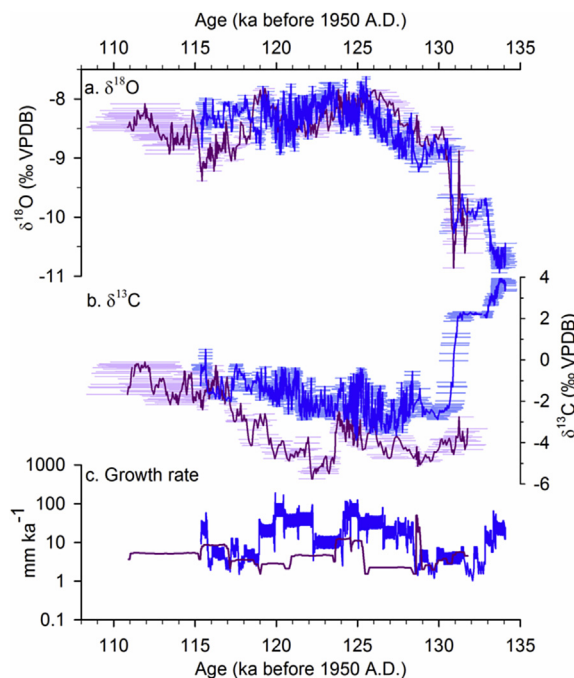


**Fig. 5.** Proxies versus time in SCH-5 (blue) and HÖL-10 (dark pink): (a)  $\delta^{18}\text{O}$ ; (b)  $\delta^{13}\text{C}$ ; (c) growth rate. Horizontal bars in (a) and (b) represent  $2\sigma$  uncertainty of the modelled ages.

warmed enough by their growth onset that surface conditions were ice-free and the epikarst was being recharged with liquid water (Spötl et al., 2002). The timing of this growth-start is synchronous within uncertainty with the initial rise in North Atlantic SSTs at  $136 \pm 2.5$  ka (Drysdale et al., 2009), which enabled evaporation and moisture transport towards the northern Alps and subsequent epikarst recharge.

The  $\delta^{18}\text{O}$  composition of SCH-5 during the first 400 years of growth is relatively stable at c.  $-10.7\text{‰}$  and also the most depleted part of the whole record (Fig. 5a). We consider that these  $\delta^{18}\text{O}$

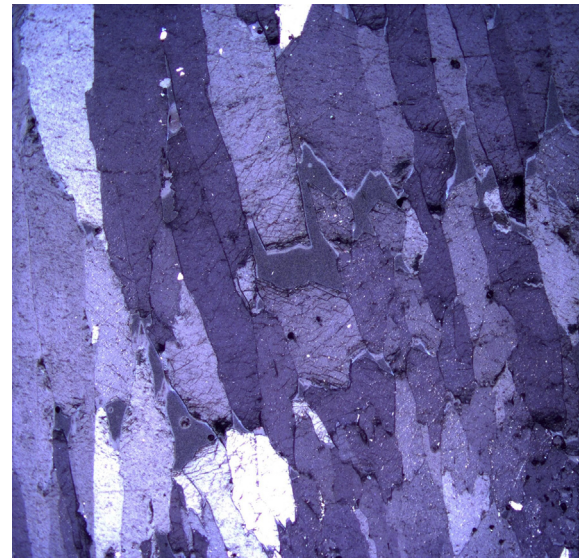


**Fig. 6.** Thin-section photomicrograph of the lowermost calcite of SCH-5 composed of columnar calcite crystals. Note lack of petrographic evidence for a change in calcite deposition in the middle part of the image (where a distinct color change can be seen macroscopically – cf. Fig. 2, which coincides with an abrupt shift in  $\delta^{18}\text{O}$  across Termination II). Growth direction is upward. Width of picture taken under cross-polarized light = 12 mm.

values during this initial growth period reflect a mixture of cool temperatures, plus a winter-dominant North Atlantic Ocean moisture source at a time when SSTs had started to rise but were still relatively low, and NADW had resumed but remained relatively weak (Drysdale et al., 2009). Under such conditions, North Atlantic moisture transported to central Europe may have had a muted summer signal and dominant winter signal as a result of extreme winter seasonality created by the expansion of North Atlantic sea ice associated with Heinrich-stadial 11 (Denton et al., 2005, 2010). Furthermore, these low  $\delta^{18}\text{O}$  values in SCH-5 correspond well to the Chinese Weak Monsoon Interval (WMI) II between  $135.5 \pm 1.0$  to  $129.0 \pm 1.0$  ka (Cheng et al., 2006), as would be expected for a time when northward surface-ocean transport of heat was limited (McManus et al., 2004).

Shifts in the stable isotopic composition of the NALPS record began with a  $1.8\text{‰}$  decrease in  $\delta^{13}\text{C}$  at  $133.7 \pm 0.5$  ka and a  $1.2\text{‰}$  increase in  $\delta^{18}\text{O}$  that led into a 2,300 year-long interstadial-type feature that contains a “saddle” in  $\delta^{18}\text{O}$  ( $-0.3\text{‰}$ ) (Figs. 5 and 7). This initial response of the SCH-5 stable isotopes is in agreement on a regional scale with shifts in speleothem  $\delta^{18}\text{O}$  recorded from Spannagel cave (Fig. 7d) (Holzkämper et al., 2004, 2005) and Corchia cave (Fig. 7e) (Drysdale et al., 2009).

The interstadial-type event is perhaps the most significant feature of our new record, as it further constrains the timing of the recovery of temperatures in Europe during TII. As AMOC strengthened and North Atlantic SSTs increased, the warmer regional atmospheric temperatures acted to enrich the  $\delta^{18}\text{O}$  of precipitating air masses in the NALPS region. In addition, the displacement of the polar front northward enabled advection of isotopically heavier Mediterranean-sourced moisture to the NALPS site. This latter hypothesis is supported by the synchronous increase in precipitation at Corchia cave in northeast Italy, as indicated by a decreasing  $\delta^{18}\text{O}$  signal during this period (Fig. 7) (Drysdale et al., 2005, 2009). Furthermore, the timing of the TII-interstadial is in agreement within uncertainty with the timing of Chinese Interstadial B.1 at  $134.5 \pm 1.0$  ka (Figs. 7 and 8), which indicates a mild strengthening of the Asian monsoon (Wang et al.,

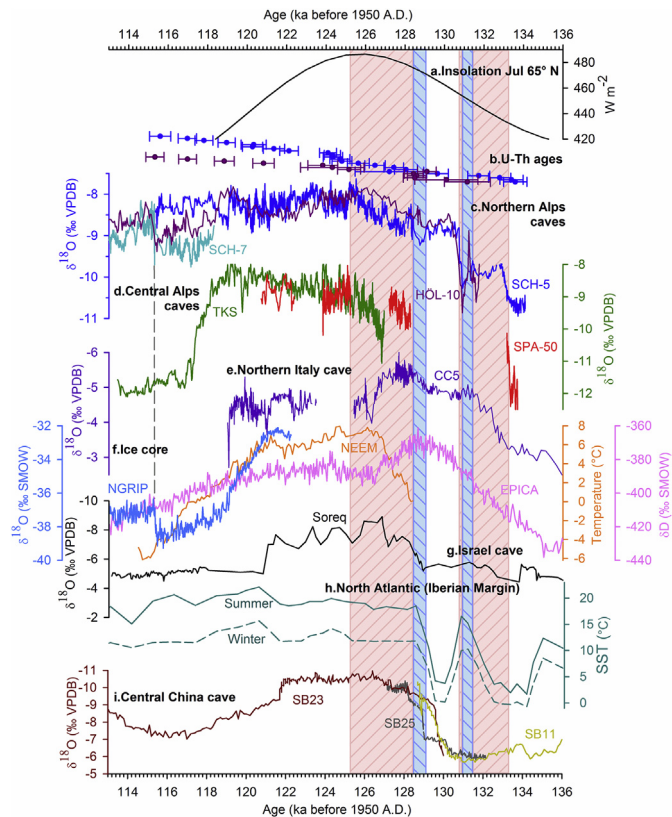


**Fig. 7.** Paleoclimate records between 136 and 113 ka: (a) July insolation at 65° N (Berger and Loutre, 1991); (b) U–Th ages with 2 $\sigma$  uncertainty for the two samples presented in this study. Blue = SCH-5. HÖL-10 = dark pink; (c)  $\delta^{18}\text{O}$  signature of northern Alpine speleothems (this study) and SCH-7 (Boch et al., 2011); (d)  $\delta^{18}\text{O}$  signature of central Alpine speleothems (SPA-50, Holzkämper et al., 2004, 2005; TKS, Meyer et al., 2008); (e)  $\delta^{18}\text{O}$  speleothem signature from Corchia cave, northern Italy (Drysdale et al., 2009); (f) Ice core records: NGRIP  $\delta^{18}\text{O}$  on the GICC05modelext timescale (Wolff et al., 2010), NEEM temperature on the EDML timescale (NEEM community members, 2013), EPICA  $\delta\text{D}$  on the EDC3 timescale (Jouzel et al., 2007); (g)  $\delta^{18}\text{O}$  speleothem signature from Soreq cave, Israel (Grant et al., 2012); (h) Iberian Margin sea-surface temperatures (Sánchez Goñi et al., 2008, 2013); (i)  $\delta^{18}\text{O}$  speleothem signature from Sanbao cave, central China (Wang et al., 2008; Cheng et al., 2009). Red and blue hatched vertical bars denote warming and cooling episodes, respectively, as defined in the SCH-5 speleothem record presented in this study.

2008; Cheng et al., 2006) in response to renewed northwards transport of oceanic heat. Cheng et al. (2009) argue that Chinese Interstadial B.1 is no more than a few hundred years in length, and this may be so for the peak-interstadial monsoon strength, however,  $\delta^{18}\text{O}$  values in the Sanbao record (Wang et al., 2008) do not return to pre-TII-interstadial values until c. 132 ka (Fig. 8a). The Chinese interstadial is thus of comparative length to the 2,300 year-long TII-interstadial witnessed in central Europe, but certainly is not as strong as the monsoon interstadials experienced during Terminations I and III (Cheng et al., 2009).

The intervening “saddle” that takes place during the middle of the TII-interstadial is manifested as a 0.3‰ decrease in  $\delta^{18}\text{O}$ . This millennial-scale event also appears to be present in the HÖL-10  $\delta^{18}\text{O}$  record (Fig. 8). First impressions would suggest that the HÖL-10 record is not synchronous with SCH-5 over the TII-interstadial, however dating uncertainties are large in this part of HÖL-10 (Table 1) and the two records agree within 2 $\sigma$  uncertainty (Fig. 5a). The amplitude of  $\delta^{18}\text{O}$  change is also greater in HÖL-10 (1.7‰) for this period, indicating (as mentioned previously) some buffering of the signal in SCH-5. The depletion in  $\delta^{18}\text{O}$  during the middle of the TII-interstadial occurs at the same time as a pause in the rise in SST and also a reduction in the amount of moisture recharge at the

Corchia cave site (Drysdale et al., 2009). The combination of a depletion in NALPS speleothem  $\delta^{18}\text{O}$ , reduction in precipitation amount in Corchia, and pause in SST rise all suggest that the TII-interstadial “saddle” may have been caused by an input of freshwater to the North Atlantic from disintegrating ice sheets. Similar to the early TII period, the freshwater would have weakened AMOC, and reduced NADW, which in turn would cool or slow down warming of SST. A reduction in NADW coincident with the TII-interstadial “saddle” is recognised in Iberian margin deep-water temperatures (Drysdale et al., 2009). As SSTs paused and NADW reduced, inhibiting the northward transfer of ocean heat, the polar front may once again have shifted southwards. Cooler temperatures, a greater proportion of North Atlantic versus Mediterranean moisture, and increased winter seasonality would have contributed to the depletion in  $\delta^{18}\text{O}$  that is the TII-interstadial “saddle”.

The TII-interstadial ended at  $131.4 \pm 0.7$  ka with another reversal in  $\delta^{18}\text{O}$  (Figs. 5 and 8), which lasted 500 years and was once again more extreme in HÖL-10 (−2.0‰) compared to SCH-5 (−0.6‰). Similar to the TII-interstadial “saddle”, this reversal coincides with a pause in the rise of SSTs, but not this time with a weakening of AMOC and reduction in NADW (Drysdale et al., 2009), which generally remained active during the last interglacial (Mokeddem et al., 2014). Rathermore, the 500-year reversal in NALPS speleothem  $\delta^{18}\text{O}$  beginning at  $131.4 \pm 0.7$  ka coincided with an increase in the abundance of the planktonic foraminifera *Turborotalita quinqueloba* at ODP site 984 south of Iceland (Fig. 8) (Oppo et al., 2006; Mokeddem et al., 2014). *T. quinqueloba* has a very shallow habitat (Simstich et al., 2003) making it a sensitive indicator of changes in the sea surface associated with the Arctic Front, defined as the

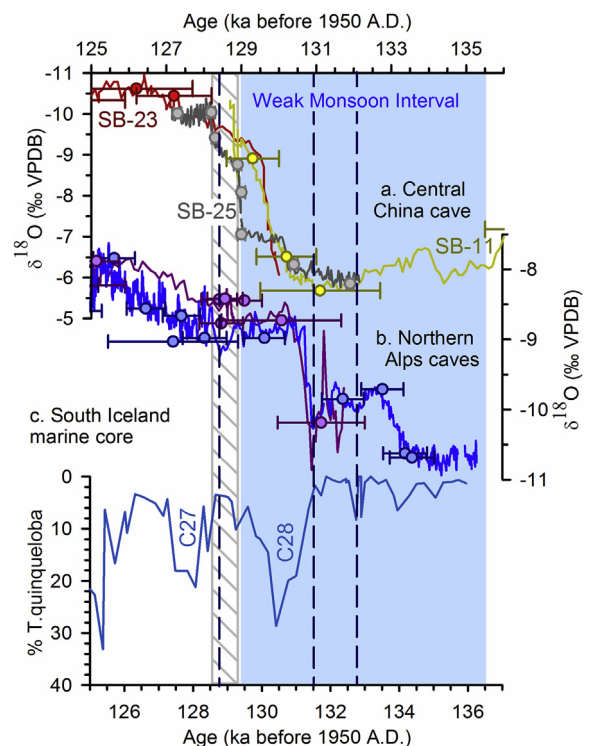


**Fig. 8.** Records of Termination II in closer detail between 125 and 137 ka. (a)  $\delta^{18}\text{O}$  of Sanbao cave, central China speleothems (Wang et al., 2008; Cheng et al., 2009). (b)  $\delta^{18}\text{O}$  from northern Alpine speleothems (this study; SCH-5, blue; HÖL-10, pink) with circles representing U–Th ages with 2 $\sigma$  uncertainty. (c). Abundance of *T. quinqueloba* at ODP site 984 south of Iceland (Mokeddem et al., 2014). Dark blue dashed vertical lines highlight three cold events identified in the SCH-5  $\delta^{18}\text{O}$  record. The Chinese weak monsoon interval is highlighted as a blue vertical bar, whilst the slowdown in monsoon strengthening is highlighted as a light grey hatched vertical bar.

boundary between the Arctic and Atlantic domains (Mokeddem et al., 2014). The peak in *T. quinqueloba* abundance indicates that the subpolar gyre had weakened, enabling cold Arctic water masses to penetrate south of Iceland, and the Arctic Front to shift in the same direction (Mokeddem et al., 2014). The North Atlantic cold anomaly known as “C28” (Fig. 8) thus had a wide impact as it is clearly recorded in the NALPS  $\delta^{18}\text{O}$  speleothem record.

The largest amplitude shift in both  $\delta^{18}\text{O}$  records (SCH-5 = +1.4‰; HÖL-10 = +2.4‰), indicating the main glacial to interglacial transition, began at  $130.9 \pm 0.9$  ka and ended at  $130.7 \pm 0.9$  ka (modelled SCH-5 ages). These ages are bracketed by SCH-5 U–Th ages of  $131.7 \pm 0.6$  and  $129.6 \pm 0.6$  ka. The rapid enrichment of  $^{18}\text{O}$  was accompanied by a 4.5‰ depletion in  $\delta^{13}\text{C}$  in SCH-5, whilst  $\delta^{13}\text{C}$  did not shift in HÖL-10 (Fig. 5b). We attribute the enrichment in  $\delta^{18}\text{O}$  over this 200 year interval to a very fast and rapid increase in regional temperature, plus a higher contribution of moisture from the Mediterranean Sea. The timing of the largest temperature change in central Europe associated with TII is in agreement with the timing of the 100-year long glacial-to-interglacial transition at 130.55 ka recorded in the varve-counted Lago Grande di Monticchio maar lake in southern Italy (Brauer et al., 2007). In addition, the main abrupt temperature rise in central Europe is in agreement with the timing of the initial strengthening of the Asian monsoon at 130.5 ka (Fig. 8a). Strengthening of the Asian monsoon thus began in parallel with the main rise in temperatures of the North Atlantic realm (Fig. 8), which would have been accompanied by an increase in evaporation and moisture advection. Such abrupt changes to the hydrological cycle are considered to be the driving force for the main shift in the  $\delta^{18}\text{O}$  of atmospheric  $\text{O}_2$  at glacial terminations, which in turn are observed as abrupt shifts in cave  $\delta^{18}\text{O}$  in monsoon regions (Cheng et al., 2009).

Following the main climate transition association with TII in central Europe,  $\delta^{18}\text{O}$  stabilised for c. 1,800 years until  $129.1 \pm 0.6$  ka, before being interrupted by a c. 600 year reversal in  $\delta^{18}\text{O}$  (SCH-5 = -0.5‰) that lasted until  $128.5 \pm 0.5$  ka. Similar to the cold reversal at  $131.4 \pm 0.7$  ka, which corresponded to the North Atlantic cold anomaly C28 (Oppo et al., 2006; Mokeddem et al., 2014), this 129 ka cold event that takes place firmly within the LIG is nearly synchronous with North Atlantic cold anomaly C27 (Fig. 8) (Oppo et al., 2006; Mokeddem et al., 2014). It is assumed that the same mechanisms which drove the 131 ka (C28) cold event were in operation for the 129 ka (C27) cold event. Furthermore, the central European cold event occurred synchronous within error with a 250-year reduction in tree pollen abundance (128.15–127.90 ka) in the Monticchio maar lake, southern Italy (Brauer et al., 2007) and also a slowdown of monsoon strengthening as recognised in Chinese speleothems (Fig. 8) (Cheng et al., 2009).

A Laurentide Ice Sheet outburst flooding event similar to the Lake Agassiz outburst flood c. 8.4 ka ago (Barber et al., 1999; Clarke et al., 2004; Leverington et al., 2002; Teller et al., 2002) is postulated to have occurred c. 126 ka ago (Nicholl et al., 2012). The early Holocene Lake Agassiz flood is considered to have forced a cold spell that is manifested in many north eastern North Atlantic records (e.g. Alley et al., 1997) including: benthic ostracod  $\delta^{18}\text{O}$  and pollen records from lakes north of the Alps (von Grafenstein et al., 1998, 1999; Tinner and Lotter, 2001); speleothem  $\delta^{18}\text{O}$  records across the Alps (Boch et al., 2009; Luetscher et al., 2012), and; studies demonstrating that some Alpine glaciers advanced during this time (e.g. Joerin et al., 2006; Nicolussi and Schlüchter, 2012). It is possible that the LIG outburst flood at c. 126 ka also led to such a climate demise (Nicholl et al., 2012). Interestingly, our central European speleothem  $\delta^{18}\text{O}$  records, which throughout TII showed a strong sensitivity to freshwater-induced cold events, does not

appear to show a distinctive cooling episode at 126 ka (Fig. 8), suggesting either that the freshwater event did not have much of an effect on North Atlantic climate, the chronology is not accurately constrained, or the event is incorrectly identified.

In summary, our new high-resolution, precisely dated central European speleothem  $\delta^{18}\text{O}$  record highlights a sequence of events across TII that includes: (a) an interstadial-type feature with an unstable climate; (b) a cold reversal; (c) the main transition associated with TII; (d) an isotopic plateau, and; (e) a cold event within the LIG. Temperature reversals during TII have long been recognised in ocean sediment records (Sarnthein and Tiedemann, 1990; Seidenkrantz et al., 1996; Chapman and Shackleton, 1998; Oppo et al., 2001; Martrat et al., 2014). In contrast, with the exception of the Asian monsoon, which records an interstadial prior to the main glacial-interglacial transition, terrestrial records have not to our knowledge revealed such details of oscillating temperatures across TII. The sequence of events associated with TII have often been compared and considered to be different to those associated with TI (e.g., Broecker and Henderson, 1998; Cheng et al., 2009; Landais et al., 2013; Martrat et al., 2014), not least because of the difference in insolation forcing. Our new high resolution, high precision  $\delta^{18}\text{O}$  speleothem record, however, improves our understanding of the sequence of events during TII in the North Atlantic realm (Fig. 9). The record demonstrates that following the large influx of meltwater and icebergs to the North Atlantic, the climate showed signs of recovery with the TII-interstadial, which was an unstable period of relatively warmer temperatures that may be analogous to Greenland Interstadial 1 (often referred to as the Bølling/Allerød) during Termination I. Furthermore, the TII-interstadial ended with a short-term cold reversal that may be akin to Greenland Stadial 1 (often referred to as the Younger Dryas). Later, once interglacial conditions were established, a centennial-scale cold reversal comparable to the widely recognised 9.2 or 8.2 ka event also occurred. The sequence of events across TII in the North Atlantic realm, i.e., interstadial-stadial-main transition,

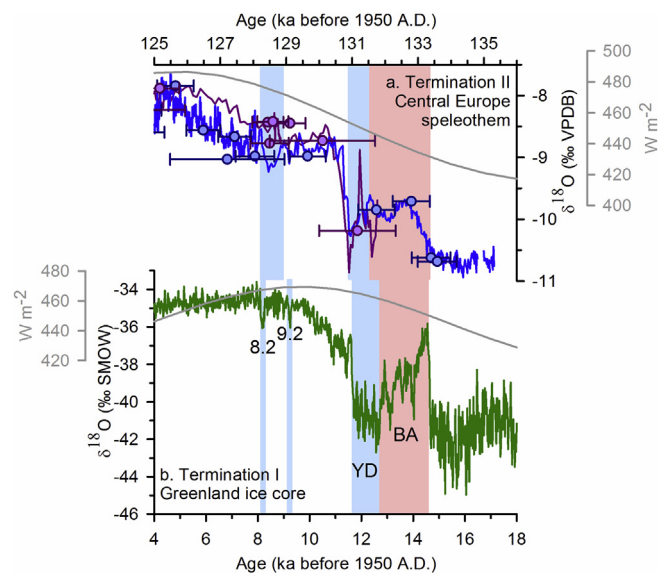


**Fig. 9.** Comparison of millennial-scale climate events during Termination I and Termination II from the North Atlantic region. (a)  $\delta^{18}\text{O}$  record of Termination II in central European speleothems, this study. (b)  $\delta^{18}\text{O}$  record of Termination I in the NGRIP ice core (North Greenland Ice Core Project members, 2004; Svensson et al., 2008). July insolation at 65° N is shown for each Termination as a grey line (Berger and Loutre, 1991). Red vertical bars highlight suborbital-scale warm intervals. Blue vertical bars highlight suborbital-scale cold intervals. BA = Bølling/Allerød. YD = Younger Dryas. 9.2 and 8.2 indicate 9.2 and 8.2 events respectively.

therefore appears to be similar to the Bølling/Allerød-Younger Dryas-main transition of T1 (Fig. 9). An important aspect here is related to the strength of the Asian monsoon. Cheng et al. (2009) demonstrated that a strong Bølling/Allerød-type interstadial, in which  $\delta^{18}\text{O}$  values were nearly comparable to interglacial ones, took place during TIII but not TII.  $\delta^{18}\text{O}$  values during the NALPS TII-interstadial remain relatively subdued in SCH-5 compared to full interglacial conditions. In contrast,  $\delta^{18}\text{O}$  values during the short interval of the TII-interstadial that is present in HÖL-10 are nearly comparable to full interglacial conditions. Whether the NALPS TII-interstadial-stadial sequence is truly analogous to the Bølling/Allerød-Younger Dryas is thus at present inconclusive and further work needs to be done to resolve this issue.

## 5. Conclusions

Precisely dated speleothem stable-isotope records from the northern rim of the European Alps document the continuous progression of temperature change through TII and the LIG. The general warming trend exhibited through TII, which started at c. 134 ka, was punctuated by a number of suborbital cold reversals that coincided with reductions in NADW formation and the migration of cold polar water southwards into the Atlantic. In addition to reducing regional air temperatures, this had the effect of shifting the polar front southwards such that the main moisture source for the northern Alps was the isotopically lighter North Atlantic. Upon resumption of NADW, regional air temperatures rose, the polar front shifted northwards, and isotopically heavier Mediterranean moisture was transported to the northern Alps. The oscillatory nature of TII and the early last interglacial that has long been recognised in deep-sea records is thus also a characteristic of terrestrial European climate.

## Acknowledgements

This work was supported by the Austrian Science Fund (FWF) project no. P222780 to CS, and in part by U.S. National Science Foundation grant 1103403 to RLE and HC. We thank Andreas Wolf and Yuri Dublyansky for assistance during field work, Manuela Wimmer for preparation and measurement of the stable isotopes, and Jerry McManus, Russell Drysdale and an anonymous reviewer for providing useful comments that helped greatly to improve the manuscript. Stable isotope data and age models for this paper are available online at NOAA's Paleoclimatology Data database.

## References

- Alley, R.B., Mayewski, P.A., Sowers, T., Stuiver, M., Taylor, K.C., Clark, P.U., 1997. Holocene climatic instability: a prominent, widespread event 8200 yr ago. *Geology* 25, 483–486. doi: 10.1130/0091-7613(1997)025<0483:HCIAPW>2.3.CO;2.
- Alley, R.B., Andrews, J.T., Brigham-Grette, J., Clarke, G.K.C., Cuffey, K.M., Fitzpatrick, J.J., Funder, S., Marshall, S.J., Miller, G.H., Mitrovica, J.X., Muhs, D.R., Otto-Bliesner, B.L., Polyak, L., White, J.W.C., 2010. History of the Greenland Ice Sheet: paleoclimatic insights. *Quat. Sci. Rev.* 29, 1728–1756. <http://dx.doi.org/10.1016/j.quascirev.2010.02.007>.
- Baker, A., Barnes, W.L., Smart, P.L., 1997. Variations in the discharge and organic matter content of stalagmites drip waters in lower cave. *Bristol. Hydrol. Proc.* 11, 1541–1555. doi: 10.1002/(SICI)1099-1085(199709)11:11<1541::AID-HYP484>3.0.CO;2-Z.
- Baldini, J.U.L., McDermott, F., Fairchild, I.J., 2006. Spatial variability in cave dripwater hydrochemistry: Implications for stalagmite paleoclimate records. *Chem. Geol.* 235, 390–404. <http://dx.doi.org/10.1016/j.chemgeo.2006.08.005>.
- Barber, D.C., Dyke, A., Hillaire-Marcel, C., Jennings, A.E., Andrews, J.T., Kerwin, M.W., Bilodeau, G., McNeely, R., Southon, J., Morehead, M.D., Gagnon, J.M., 1999. Forcing of the cold event of 8,200 years ago by catastrophic drainage of Laurentide lakes. *Nature* 400, 344–348. <http://dx.doi.org/10.1038/22504>.
- Bauch, H.A., Erlenkeuser, H., Jung, S.J.A., Thiede, J., 2000. Surface and deep water changes in the subpolar North Atlantic during Termination II and the Last Interglaciation. *Paleoceanography* 15, 76–84. <http://dx.doi.org/10.1029/1998PA000343>.
- Berger, A., Loutre, M.F., 1991. Insolation values for the climate of the last 10 million years. *Quat. Sci. Rev.* 10, 297–317. [http://dx.doi.org/10.1016/0277-3791\(91\)90033-Q](http://dx.doi.org/10.1016/0277-3791(91)90033-Q).
- Berger, A., Yin, Q.Z., 2012. Modelling the past and future interglacials in response to astronomical and greenhouse gas forcing. In: Henderson-Sellers, A., McGuffie, K. (Eds.), *The Future of the World's Climate*. Elsevier, Amsterdam, pp. 1123–1161.
- Bintanja, R., van de Wal, R.S.W., Oerlemans, J., 2005. Modelled atmospheric temperatures and global sea levels over the past million years. *Nature* 437, 125–128. <http://dx.doi.org/10.1038/nature03975>.
- Boch, R., Spötl, C., Kramers, J., 2009. High-resolution isotope records of early Holocene rapid climate change from two coeval stalagmites of Katerloch Cave, Austria. *Quat. Sci. Rev.* 28, 2527–2538. <http://dx.doi.org/10.1016/j.quascirev.2009.05.015>.
- Boch, R., Cheng, H., Spötl, C., Edwards, R.L., Wang, X., Häuselmann, Ph., 2011. NALPS: a precisely dated European climate record 120–60 ka. *Clim. Past* 7, 1247–1259. <http://dx.doi.org/10.5194/cp-7-1247-2011>.
- Bond, G., Heinrich, H., Broecker, W., Labeyrie, L., McManus, J., Andrews, J., Huon, S., Jantschik, R., Clasen, S., Simet, C., Tedesco, K., Klas, M., Bonani, G., Ivy, S., 1992. Evidence for massive discharges of icebergs into the North Atlantic ocean during the last glacial period. *Nature* 360, 245–249.
- Bond, G., Kromer, B., Beer, J., Muscheler, R., Evans, M.N., Showers, W., Hoffmann, S., Lotti-Bond, R., Hajdas, I., Bonani, G., 2001. Persistent solar influence on North Atlantic climate during the Holocene. *Science* 294, 2130–2136. <http://dx.doi.org/10.1126/science.1065680>.
- Brauer, A., Allen, J.R.M., Mingram, J., Dulski, P., Wulf, S., Huntley, B., 2007. Evidence for last interglacial chronology and environmental change from Southern Europe. *Proc. Natl. Acad. Sci. U. S. A.* 104, 450–455. <http://dx.doi.org/10.1073/pnas.0603321104>.
- Broecker, S., Henderson, G.M., 1998. The sequence of events surrounding Termination II and their implications for the cause of glacial-interglacial  $\text{CO}_2$  changes. *Paleocean* 13, 352–364. <http://dx.doi.org/10.1029/98PA00920>.
- Bronk Ramsey, C., 2008. Deposition models for chronological records. *Quat. Sci. Rev.* 27, 42–60. <http://dx.doi.org/10.1016/j.quascirev.2007.01.019>.
- Bronk Ramsey, C., Lee, S., 2013. Recent and planned developments of the program OxCal. *Radiocarbon* 55, 720–730. [http://dx.doi.org/10.2458/azu\\_js\\_rc.55.16215](http://dx.doi.org/10.2458/azu_js_rc.55.16215).
- CAPE-Last Interglacial Project Members, 2006. Last Interglacial Arctic warmth confirms polar amplification of climate change. *Quat. Sci. Rev.* 25, 1383–1400. <http://dx.doi.org/10.1016/j.quascirev.2006.01.033>.
- Chapman, M.R., Shackleton, N.J., 1998. Millennial-scale fluctuations in North Atlantic heat flux during the last 150,000 years. *Earth Planet Sci. Lett.* 159, 57–70. [http://dx.doi.org/10.1016/S0012-821X\(98\)00068-5](http://dx.doi.org/10.1016/S0012-821X(98)00068-5).
- Cheng, H., Edwards, R.L., Wang, Y., Kong, X., Ming, Y., Kelly, M.J., Wang, X., Gallup, C.D., Liu, W., 2006. A penultimate glacial monsoon record from Hulu Cave and two-phase glacial terminations. *Geology* 34, 217–220. <http://dx.doi.org/10.1130/G22289.1>.
- Cheng, H., Edwards, R.L., Broecker, W.S., Denton, G.H., Kong, X., Wang, Y., Zhang, R., Wang, X., 2009. Ice age terminations. *Science* 326, 248–252. <http://dx.doi.org/10.1126/science.1177840>.
- Cheng, H., Edwards, R.L., Shen, C.-C., Polyak, V.J., Asmerom, Y., Woodhead, J., Hellstrom, J., Wang, Y., Kong, X., Spötl, C., Wang, X., Calvin Alexander Jr., E., 2013. Improvements in  $^{230}\text{Th}$  dating,  $^{230}\text{Th}$  and  $^{234}\text{U}$  half-life values, and U-Th isotopic measurements by multi-collector inductively coupled plasma mass spectrometry. *Earth Planet Sci. Lett.* 371–372, 82–91. <http://dx.doi.org/10.1016/j.epsl.2013.04.006>.
- Clarke, G.K.C., Leverington, D.W., Taylor, J.T., Dyke, A.S., 2004. Paleohydrology of the last outburst flood from glacial lake Agassiz and the 8200 BP cold event. *Quat. Sci. Rev.* 23, 389–407. <http://dx.doi.org/10.1016/j.quascirev.2003.06.004>.
- Denton, G.H., Alley, R.B., Comer, G.C., Broecker, W.S., 2005. The role of seasonality in abrupt climate change. *Quat. Sci. Rev.* 24, 1159–1182. <http://dx.doi.org/10.1016/j.quascirev.2004.12.002>.
- Denton, G.H., Anderson, R.F., Toggweiler, J.R., Edwads, R.L., Schaefer, J.M., Putnam, A.E., 2010. The last glacial termination. *Science* 328, 1652–1656. <http://dx.doi.org/10.1126/science.1184119>.
- Dorale, J.A., Liu, Z., 2009. Limitations of hendi test criteria in judging the paleoclimatic suitability of speleothems and the need for replication. *J. Cave Karst Stud.* 71, 73–80.
- Drysdale, R.N., Zanchetta, G., Hellstrom, J.C., Fallick, A.E., Zhao, J.-X., 2005. Stalagmite evidence for the onset of the Last Interglacial in southern Europe at  $129 \pm 1$  ka. *Geophys. Res. Lett.* 32, L24708. <http://dx.doi.org/10.1029/2005GL024658>.
- Drysdale, R.N., Hellstrom, J.C., Zanchetta, G., Fallick, A.E., Sánchez Goñi, M.F., Couchoud, I., McDonald, J., Maas, J., Lohmann, G., Isola, I., 2009. Evidence for obliquity forcing of glacial termination II. *Science* 325, 1527–1531. <http://dx.doi.org/10.1126/science.1170371>.
- Dutton, A., Lambeck, K., 2012. Ice volume and sea level during the last interglacial. *Science* 337, 216–219. <http://dx.doi.org/10.1126/science.1205749>.
- Field, R.D., 2010. Observed and modelled controls on precipitation  $\delta^{18}\text{O}$  over Europe: from local temperature to the Northern Annual Mode. *J. Geophys. Res.* 115, D12101. <http://dx.doi.org/10.1029/2009JD013370>.
- FreeVectorMaps.com, 2014. Map of Globe of Middle East- Single Color, Available from Free Vector Maps. <http://freevectormaps.com>.
- Gouzy, A., Malaize, B., Pujol, C., Charlier, K., 2004. Climatic “pause” during Termination II identified in shallow and intermediate waters off the Iberian margin. *Quat. Sci. Rev.* 23, 1523–1528. <http://dx.doi.org/10.1016/j.quascirev.2004.03.002>.

- Grant, K.M., Rohling, E.J., Bar-Matthews, M., Ayalon, A., Medina-Elizalde, M., Bronk Ramsey, C., Satow, C., Roberts, P., 2012. Rapid coupling between ice volume and polar temperature over the past 150,000 years. *Nature* 491, 744–747. <http://dx.doi.org/10.1038/nature11593>.
- Heinrich, H., 1988. Origin and consequences of cyclic ice rafting in the Northeast Atlantic Ocean during the past 130,000 years. *Quat. Res.* 29, 142–152. [http://dx.doi.org/10.1016/0033-5894\(88\)90057-9](http://dx.doi.org/10.1016/0033-5894(88)90057-9).
- Hendy, C.H., 1971. The isotope geochemistry of speleothems—I. The calculation of the effects of different modes of formation on the isotopic composition of speleothems and their applicability as paleoclimatic indicators. *Geochim. Cosmochim. Acta* 35, 801–824. [http://dx.doi.org/10.1016/0016-7037\(71\)90127-X](http://dx.doi.org/10.1016/0016-7037(71)90127-X).
- Holzkmper, S., Mangini, A., Spötl, C., Mudelsee, M., 2004. Timing and progression of the Last Interglacial derived from a high alpine stalagmite. *Geophys. Res. Lett.* 31, L07201. <http://dx.doi.org/10.1029/2003GL019112>.
- Holzkmper, S., Spötl, C., Mangini, A., 2005. High-precision constraints on timing of Alpine warm periods during the middle to late Pleistocene using speleothem growth periods. *Earth Planet. Sci. Lett.* 236, 751–764. <http://dx.doi.org/10.1016/j.epsl.2005.06.002>.
- Humer, G., Rank, D., Trimborn, P., Stichter, W., 1995. Niederschlagsisotopenmessnetz Österreich. In: *Monographien*, vol. 52. Umweltbundesamt, Vienna.
- Jaffey, A.H., Flynn, K.F., Glendenin, L.E., Bentley, W.C., Essling, A.M., 1971. Precision measurement of half-lives and specific activities of  $^{235}\text{U}$  and  $^{238}\text{U}$ . *Phys. Rev. C* 4, 1889. <http://dx.doi.org/10.1103/PhysRevC.4.1889>.
- Joerin, U.J., Stocker, T.F., Schlüchter, C., 2006. Multicentury glacier fluctuations in the Swiss Alps during the Holocene. *Holocene* 16, 697–704. <http://dx.doi.org/10.1191/0959683606h1964p>.
- Jouzel, J., Masson-Delmotte, V., Cattani, O., Dreyfus, G., Falourd, S., Hoffmann, G., Minster, B., Nouet, J., Barnola, J.M., Chappellaz, J., Fischer, H., Gallet, J.C., Johnsen, S., Leuenberger, M., Loulergue, L., Luethi, D., Oerter, H., Parrenin, F., Raisbeck, G., Raynaud, D., Schilt, A., Schwander, J., Selmo, E., Souchez, R., Spahni, R., Stauffer, B., Steffensen, J.P., Stenni, B., Stocker, T.F., Tison, J.L., Werner, M., Wolff, E.W., 2007. Orbital and millennial Antarctic climate variability over the past 800,000 years. *Science* 317, 793–797. <http://dx.doi.org/10.1126/science.1141038>.
- Kaiser, A., Scheiffinger, H., Kralik, M., Papesch, W., Rank, D., Stichter, W., 2002. Links Between Meteorological Conditions and Spatial/temporal Variations in Long-term Isotopic Records from the Austrian Precipitation Network, in Study of Environmental Change Using Isotope Techniques, C&S Paper Series 13/P. International Atomic Energy Agency, pp. 67–76.
- Kaspar, F., Kuhl, N., Cubasch, U., Litt, T., 2005. A model-data comparison of European temperatures in the Eemian interglacial. *Geophys. Res. Lett.* 32, L11703. <http://dx.doi.org/10.1029/2005GL022456>.
- Koerner, R.M., 1989. Ice core evidence for extensive melting of the Greenland ice sheet in the last interglacial. *Science* 244, 964–968. <http://dx.doi.org/10.1126/science.244.4907.964>.
- Kopp, R.E., Simons, F.J., Mitrovica, J.X., Maloof, A.C., Oppenheimer, M., 2009. Probabilistic assessment of sea level during the last interglacial stage. *Nature* 462. <http://dx.doi.org/10.1038/nature08686>, 863–U851.
- Landais, A., Dreyfus, G., Capron, E., Jouzel, J., Masson-Delmotte, V., Roche, D.M., Prié, F., Caillon, N., Chappellaz, J., Leuenberger, M., Lourantou, A., Parrenin, F., Raynaud, D., Teste, G., 2013. Two-phase change in  $\text{CO}_2$ , Antarctic temperature and global climate during Termination II. *Nat. Geosci.* 6, 1062–1065. <http://dx.doi.org/10.1038/ngeo1985>.
- Lauber, U., Goldscheider, N., 2014. Use of artificial and natural tracers to assess groundwater transit-time distribution and flow systems in a high-alpine karst system (Wetterstein Mountains, Germany). *Hydrogeol. J.* 22, 1807–1824. <http://dx.doi.org/10.1007/s10040-014-1173-6>.
- LeGrande, A.N., Schmidt, G.A., 2006. Global gridded data set of the oxygen isotopic composition in seawater. *Geophys. Res. Lett.* 33, L12604. <http://dx.doi.org/10.1029/2006GL026011>.
- Leverington, D.W., Mann, J.D., Teller, J.T., 2002. Changes in the bathymetry and volume of glacial Lake Agassiz between 9200 and 7700  $^{14}\text{C}$  yr B.P. *Quat. Res.* 57, 244–252. <http://dx.doi.org/10.1006/qres.2001.2311>.
- Luetscher, M., Hoffmann, D.L., Müller, W., Spötl, C., 2012. The 8.2 ka event in the northern Alps. *Geophys. Res. Abstr.* 14, EGU2012–10425.
- Luetscher, M., Hunkeler, D., Müller, W., Spötl, C., 2014. Integrating drip-water chemistry and speleothem proxy data in a ventilated cave system, Bärenhöhle, Austria. *Geophys. Res. Abstr.* 16, EGU2014–10761-1.
- Luetscher, M., Boch, R., Sodemann, H., Spötl, C., Cheng, H., Edwards, R.L., Frisia, S., Hof, F., Müller, W., 2015. North Atlantic storm track changes during the Last Glacial Maximum recorded by Alpine speleothems. *Nat. Comm.* 6, 1–6. <http://dx.doi.org/10.1038/ncomms7344>.
- Mangini, A., Verdes, P., Spötl, C., Scholz, D., Vollweiler, N., Kromer, B., 2007. Persistent influence of the North Atlantic hydrography on Central European winter temperature during the last 9,000 years. *Geophys. Res. Lett.* 34, L02704. <http://dx.doi.org/10.1029/2006GL028600>.
- Martrat, B., Jimenez-Amat, P., Zahn, R., Grimalt, J.O., 2014. Similarities and dissimilarities between the last two deglaciations and Interglaciations in the North Atlantic region. *Quat. Sci. Rev.* 99, 122–134. <http://dx.doi.org/10.1016/j.quascirev.2014.06.016>.
- McManus, J.F., Bond, G.C., Broecker, W.S., Johnsen, S., Labeyrie, L., Higgins, S., 1994. High-resolution climate records from the North Atlantic during the last interglacial. *Nature* 371, 326–329. <http://dx.doi.org/10.1038/371326a0>.
- McManus, J.F., Anderson, R.F., Broecker, W.S., Fleisher, M.Q., Higgins, S.M., 1998. Radiometrically determined sedimentary fluxes in the sub-polar North Atlantic during the last 140,000 years. *Earth Planet. Sci. Lett.* 155, 29–43. [http://dx.doi.org/10.1016/S0012-821X\(97\)00201-X](http://dx.doi.org/10.1016/S0012-821X(97)00201-X).
- McManus, J.F., Oppo, D.W., Cullen, J.L., 1999. A 0.5-Million-Year record of millennial-scale climate variability in the North Atlantic. *Science* 283, 971–975. <http://dx.doi.org/10.1126/science.283.5404.971>.
- McManus, J.F., Francois, R., Gherardi, J.-M., Keigwin, L.D., Brown-Leger, S., 2004. Collapse and rapid resumption of Atlantic meridional circulation linked to deglacial climate changes. *Nature* 428, 834–837. <http://dx.doi.org/10.1038/nature02494>.
- Meyer, M., Spötl, C., Mangini, A., 2008. The demise of the Last Interglacial recorded in isotopically dated speleothems from the Alps. *Quat. Sci. Rev.* 27, 476–496. <http://dx.doi.org/10.1016/j.quascirev.2007.11.005>.
- Mokeddem, Z., McManus, J.F., Oppo, D.W., 2014. Oceanographic dynamics and the end of the last interglacial in the subpolar North Atlantic. *Proc. Natl. Acad. Sci. U. S. A.* 111, 11263–11268. <http://dx.doi.org/10.1073/pnas.1322103111>.
- Moseley, G.E., Spötl, C., Svensson, A., Cheng, H., Brandstätter, S., Edwards, R.L., 2014. Multi-speleothem record reveals tightly coupled climate between Central Europe and Greenland during MIS 3. *Geology* 42, 1043–1046. <http://dx.doi.org/10.1130/G36063.1>.
- NEEM community members, 2013. Eemian interglacial reconstructed from a Greenland folded ice core. *Nature* 493, 489–493. <http://dx.doi.org/10.1038/nature11789>.
- Nicholl, J.A.L., Hodell, D.A., David, B., Naafs, A., Hillaire-Marcel, C., Channell, J.E.T., Romero, O.E., 2012. A Laurentide outburst flooding event during the last interglacial period. *Nat. Geosci.* 5, 901–902. <http://dx.doi.org/10.1038/NGEO1622>.
- Nicolussi, J., Schlüchter, C., 2012. The 8.2 ka event – calendar-dated glacier response in the Alps. *Geology* 40, 819–822. <http://dx.doi.org/10.1130/G32406.1>.
- North Greenland Ice Core Project Members, 2004. High-resolution record of Northern Hemisphere climate extending into the last interglacial period. *Nature* 431, 147–151. <http://dx.doi.org/10.1038/nature02805>.
- Oppo, D.W., Keigwin, L.D., McManus, J.F., Cullen, J.L., 2001. Persistent suborbital climate variability in marine isotope stage 5 and Termination II. *Paleoceanography* 16, 280–292. <http://dx.doi.org/10.1029/2000PA000527>.
- Oppo, D.W., McManus, J.F., Cullen, J.L., 2006. Evolution and demise of the Last Interglacial warmth in the subpolar North Atlantic. *Quat. Sci. Rev.* 25, 3268–3277. <http://dx.doi.org/10.1016/j.quascirev.2006.07.006>.
- Otto-Bliesner, B.L., Marshall, S.J., Overpeck, J.T., Miller, G.H., Hu, A., C. L. I. P. members, 2006. Simulating arctic climate warmth and icefield retreat in the Last Interglacial. *Science* 311, 1751–1753. <http://dx.doi.org/10.1126/science.1120808>.
- Sánchez Goñi, M.F., Eynaud, F., Turon, J.L., Shackleton, N.J., 1999. High resolution palynological record of the Iberian margin: direct land-sea correlation for the Last Interglacial complex. *Earth Planet. Sci. Lett.* 171, 123–137. [http://dx.doi.org/10.1016/S0012-821X\(99\)00141-7](http://dx.doi.org/10.1016/S0012-821X(99)00141-7).
- Sánchez Goñi, M.F., Landais, A., Fletcher, W., Naughton, F., Desprat, A., Duprat, J., 2008. Contrasting impacts of Dansgaard-Oeschger events over a western European latitudinal transect modulated by orbital parameters. *Quat. Sci. Rev.* 27, 1136–1151. <http://dx.doi.org/10.1016/j.quascirev.2008.03.003>.
- Sánchez Goñi, M.F., Bard, E., Landais, A., Rossignol, L., d'Errico, F., 2013. Increased air-sea thermal gradient during the last interglacial/glacial transition. *Nat. Geosci.* 6, 837–841. <http://dx.doi.org/10.1038/ngeo1924>.
- Sarnthein, M., Tiedemann, R., 1990. Younger Dryas-style cooling events at glacial terminations I–VI at ODP Site 658: associated benthic  $\delta^{13}\text{C}$  anomalies constrain meltwater hypothesis. *Paleoceanography* 5, 1041–1055. <http://dx.doi.org/10.1029/PA005i006p01041>.
- Schürch, M., Kozel, R., Schotterer, U., Tripet, J.-P., 2003. Observation of isotopes in the water cycle—the Swiss National Network (NISOT). *Environ. Geol.* 45, 1–11. <http://dx.doi.org/10.1007/s00254-003-0843-9>.
- Seidenkrantz, M.-S., Bornmalm, L., Johnsen, S.J., Knudsen, K.L., Kuijpers, A., Lauritzen, S.-E., Leroy, S.A.G., Mergel, I., Schweger, C., Van Vliet-Lanoë, B., 1996. Two-step deglaciation at the oxygen isotope stage 6/5e transition: the Zeifen-Kattegat climate oscillation. *Quat. Sci. Rev.* 15, 63–75. [http://dx.doi.org/10.1016/0277-3791\(95\)00086-0](http://dx.doi.org/10.1016/0277-3791(95)00086-0).
- Shen, C.-C., Wu, C.-C., Cheng, H., Edwards, R.L., Hsieh, Y.-T., Gallet, S., Chang, C.-C., Li, T.-Y., Lam, D.D., Kano, A., Hori, M., Spötl, C., 2012. High-precision and high-resolution carbonate  $^{230}\text{Th}$  dating by MC-ICP-MS with SEM protocols. *Geochim. Cosmochim. Acta* 99, 71–86. <http://dx.doi.org/10.1016/j.gca.2012.09.018>.
- Simstich, J., Sarnthein, M., Erlenkeuser, H., 2003. Paired  $\delta^{18}\text{O}$  signals of *Neogloboquadrina pachyderma* (s) and *Turborotalita quinqueloba* show thermal stratification structure in Nordic Seas. *Mar. Micropaleontol.* 48, 107–125. [http://dx.doi.org/10.1016/S0377-8398\(02\)00165-2](http://dx.doi.org/10.1016/S0377-8398(02)00165-2).
- Smart, P.L., Friederich, H., 1986. Water movement and storage in the unsaturated zone of a maturely karstified carbonate aquifer, Mendip Hills, England. In: *Proceedings of the Environmental Problems in Karst Terranes and Their Solutions Conference*, October, Bowling Green, Kentucky, pp. 59–87.
- Sodemann, H., 2006. Tropospheric Transport of Water Vapour: Lagrangian and Eulerian Perspectives. Ph.D. thesis. Swiss Federal Institute of Technology, Zurich, p. 225.
- Sodemann, H., Zubler, E., 2010. Seasonal and inter-annual variability of the moisture sources for Alpine precipitation during 1995–2002. *Int. J. Climatol.* 30, 947–961. <http://dx.doi.org/10.1002/joc.1932>.
- Spötl, C., Mangini, A., Frank, N., Eichstädter, R., Burns, S.J., 2002. Start of the last interglacial period at 135 ka: evidence from a high Alpine speleothem. *Geology* 30, 815–818.

- Spötl, C., 2011. Long-term performance of the Gasbench isotope ratio mass spectrometry system for the stable isotope analysis of carbonate microsamples. *Rapid Commun. Mass Spectrom.* 25, 1683–1685. <http://dx.doi.org/10.1002/rcm.5037>.
- Spötl, C., Boch, R., Wolf, A., 2011. Eiszeitliche Klimadynamik im Spiegel eines Sta-lagmiten aus dem Hölloch (Bayern/Vorarlberg). *Die Höhle* 62, 46–53.
- Stocker, T.F., Qin, D., Plattner, G.-K., Tignor, M., Allen, S.K., Boschung, J., Nauels, A., Xia, Y., Bex, V., Midgley, P.M. (Eds.), 2013. *IPCC, 2013: Climate Change 2013: the Physical Science Basis. Contribution of Working Group I to the Fifth Assessment Report of the Intergovernmental Panel on Climate Change*. Cambridge University Press, Cambridge.
- Stone, E.J., Lunt, D.J., Annan, J.D., Hargreaves, J.C., 2013. Quantification of the Greenland ice sheet contribution to Last Interglacial sea level rise. *Clim. Past* 9, 621–639. <http://dx.doi.org/10.5194/cp-9-621-2013>.
- Svensson, A., Anderson, K.K., Bigler, M., Clausen, H.B., Dahl-Jensen, D., Davies, S.M., Johnsen, S.J., Muscheler, R., Perrenin, F., Rasmussen, S.O., Röthlisberger, R., Seierstad, I., Steffensen, J.P., Vinther, B.M., 2008. A 60000 year stratigraphic ice core chronology. *Clim. Past* 4, 47–57. <http://dx.doi.org/10.5194/cp-4-47-2008>.
- Teller, J.T., Leverington, D.W., Mann, J.D., 2002. Freshwater outbursts to the oceans from glacial Lake Agassiz and their role in climate change during the last deglaciation. *Quat. Sci. Rev.* 21, 879–887. [http://dx.doi.org/10.1016/S0277-3791\(01\)00145-7](http://dx.doi.org/10.1016/S0277-3791(01)00145-7).
- Thompson, W.G., Allen Curran, H., Wilson, M.A., White, B., 2011. Sea-level oscillations during the last interglacial highstand recorded by Bahamas corals. *Nat. Geosci.* 4, 684–687. <http://dx.doi.org/10.1038/ngeo1253>.
- Tinner, W., Lotter, A.F., 2001. Central European vegetation response to abrupt climate change at 8.2 ka. *Geology* 29, 551–554 doi: 10.1130/0091-7613(2001)029<0551:CEVRTA>2.0.CO;2.
- von Grafenstein, U., Erlenkeuser, H., Müller, J., Jouzel, J., Johnsen, S., 1998. The cold event 8200 years ago documented in oxygen isotope records of precipitation in Europe and Greenland. *Clim. Dyn.* 14, 73–81. <http://dx.doi.org/10.1007/s003820050210>.
- von Grafenstein, U., Erlenkeuser, H., Brauer, A., Jouzel, J., Johnsen, S.J., 1999. A mid-European decadal isotope-climate record from 15,500 to 5000 years B.P. *Science* 284, 1654–1657. <http://dx.doi.org/10.1126/science.284.5420.1654>.
- van Husen, D., 1987. *Die Ostalpen und ihr Vorland in der letzten Eiszeit (Würm). Map 1: 500,000, Vienna (Geol. Bundesanstalt, Vienna)*.
- Waelbroeck, C., Frank, N., Jouzel, J., Parrenin, F., Masson-Delmonte, V., Genty, D., 2008. Transferring radiometric dating of the last interglacial sea level high stand to marine and ice core records. *Earth Planet. Sci. Lett.* 265, 183–194. <http://dx.doi.org/10.1016/j.epsl.2007.10.006>.
- Wang, Y., Cheng, H., Edwards, R.L., Kong, X., Shao, X., Chen, S., Wu, J., Jiang, X., Wang, X., An, Z., 2008. Millennial- and orbital-scale changes in the East Asian monsoon over the past 224,000 years. *Nature* 451, 1090–1093. <http://dx.doi.org/10.1038/nature06692>.
- Wedepohl, K.H., 1995. The composition of the continental crust. *Geochim. Cosmochim. Acta* 59, 1217–1239. [http://dx.doi.org/10.1016/0016-7037\(95\)00038-2](http://dx.doi.org/10.1016/0016-7037(95)00038-2).
- Wolff, E.W., Chappellaz, J., Blunier, T., Rasmussen, S.O., Svensson, A., 2010. Millennial-scale variability during the last glacial: the ice core record. *Quat. Sci. Rev.* 29, 2828–2838. <http://dx.doi.org/10.1016/j.quascirev.2009.10.013>.